INTERNATIONAL
Agrophysics
www.international-agrophysics.org

Int. Agrophys., 2024, 38, 407-422
doi: 10.31545/intagr/192302

Evaluating vegetation dynamics in the Yangtze river basin in relation to climatological parameters using remote sensing data from 2001 to 2022

Jiwu Li[1], *Xiaohong Zhang*[2], *Iman Rousta*[3,4]*, *Haraldur Olafsson*[4], *Jaromir Krzyszczak*[5]

[1]Forestry and Garden, Longde County Forestry Grassland Development Center, Debang Road, Liupanshan Str., Longde County, Ningxia, 756300, China
[2]Garden Engineering, Ningxia Zefeng Construction Engineering Co., LTD., Ningxia Longde County Scholar World, 756300, China
[3]Department of Geography, Yazd University, Yazd 8915818411, Iran
[4]Institute for Atmospheric Sciences, Weather and Climate and Department of Physics, University of Iceland and Icelandic Meteorological Office (IMO), Bustadavegur 7, IS-108 Reykjavik, Iceland
[5]Institute of Agrophysics, Polish Academy of Sciences, Doświadczalna 4, 20-290 Lublin, Poland

Received July 25, 2024; accepted August 13, 2024

A b s t r a c t. This study investigates the dynamics of vegetation cover in the Yangtze river basin, separated into three sub-basins: upper basin, middle basin, and lower basin, concerning temperature and precipitation changes. The variations in the normalized difference vegetation index, precipitation, and temperature over 22 years (2001-2022) were analyzed annually, seasonally, and monthly using remote sensing data. The relationship between normalized difference vegetation index changes and precipitation and temperature was evaluated using Kendall's correlation. The findings reveal a significant correlation between vegetation, surface temperature, and precipitation in the Yangtze river basin. Additionally, a significant (at p-value = 0.05) downward trend of vegetation coverage in the entire basin was observed for the classes between 0.2 and 0.5 (indicating poor and moderate vegetation). Conversely, a significant (at p-value = 0.05) upward trend in the area covered by denser vegetation (normalized difference vegetation index exceeding 0.5) was observed during the studied period in the Yangtze river basin. The largest vegetation coverage area was observed in middle basin, while the lowest values were seen in upper basin in 2008, middle basin in 2001, and lower basin in 2005. The highest vegetation coverage area in all three basins was recorded in 2021. In general, a significant (at p-value = 0.01) upward trend in vegetation coverage was observed in all three basins between 2001 and 2022. Finally, the results demonstrate that temperature exhibits a stronger correlation with increased vegetation cover in the Yangtze river basin, compared to precipitation.

K e y w o r d s: normalized difference vegetation index, land surface temperature, precipitation, vegetation coverage, Yangtze river basin, remote sensing

1. INTRODUCTION

One of the most critical aspects of vegetation management and control for sustainable development is investigating the sustainable process of vegetation change. Vegetation refers to the various types of trees, fodder, bushes, grass, and vegetables that grow on the Earth's surface (Cheng *et al.*, 2024; Wang *et al.*, 2024; Xie *et al.*, 2023). The absence of vegetation on the ground stands as a significant factor contributing to soil surface erosion caused by rain and other factors (Zhang *et al.*, 2022, 2023; Liu *et al.*, 2024; Zhao *et al.*, 2024). Vegetation serves as the crucial interface between the atmosphere, soil, and water within terrestrial ecosystems (Kafarski *et al.*, 2019; Majcher *et al.*, 2021; Li *et al.*, 2024). Through such processes as photosynthesis, evaporation, and transpiration, it plays a vital role in regulating the global carbon cycle, water cycle, energy exchange, and global climate stability (Guo *et al.*, 2014; Xu *et al.*, 2022; Zhou *et al.*, 2023a, b; Chen *et al.*, 2023). Given that alterations in vegetation cover can disrupt ecosystem conditions and functioning, the study of vegetation dynamics has become a pressing environmental concern, requiring both temporal and mechanistic investigations (Rannow and Neubert, 2014). Various factors drive changes in vegetation over time and impact ecosystem conditions and functioning. These factors encompass human activities,

*Corresponding author e-mail: irousta@yazd.ac.ir

such as land use changes and management practices like vegetation revitalization, as well as natural influences like rainfall, temperature, and weather events (such as droughts, floods, fires, *etc*.) (Tang *et al.*, 2020). Precipitation, in particular, plays a pivotal role in the growth and decline of vegetation. When rainfall is insufficient, vegetation starts to dwindle, and if temperatures rise while strong winds blow and relative humidity decreases, drought severity increases, subsequently leading to a more rapid decline in vegetation within an area (Katiraie Boroujerdy, 2016). The normalized difference vegetation index (NDVI), as a fundamental measure, stands out as one of the most extensively employed indices for examining vegetation changes (Kundu *et al.*, 2016). Analyzing the trend of this index carries significance in numerous scenarios, encompassing ecological assessments in response to global warming and desertification (Zhang *et al.*, 2013). Consequently, monitoring the dynamics of biological vegetation is crucial in deepening our understanding and enhancing feedback mechanisms between vegetation and the atmosphere (Angelini *et al.*, 2011). The vegetation index represents one of the frequently utilized measures, calculated based on the disparities between red and infrared bands near vegetation. It offers valuable insights into seasonal and annual variations in vegetation (Tucker and Choudhury, 1987; Hu *et al.*, 2019). Traditional methods for investigating vegetation changes are often time-consuming and resource-intensive. Conversely, the challenges in obtaining precise historical vegetation location data and ensuring its continuous availability have prompted experts to seek faster, more accurate, and cost-effective approaches. Therefore, the utilization of the satellite information technology may hold advantages over other methods (Aronoff, 2004). Leveraging remote sensing, especially from the satellite level, and long-term time-series data analyses proves to be the most suitable approach for assessing the evolution in the processes governing the natural and anthropogenic phenomena (Sun *et al.*, 2024; Gu *et al.*, 2024).

Remote sensing images and technology provide a globally valuable tool for studying natural and human-induced phenomena (Yu and Zhou, 2024; Yin *et al.*, 2023a, b; Luo *et al.*, 2024). In recent years, numerous studies have been conducted for the Central Asia region to explore the dynamics and processes of plant changes, recognized as a pivotal influence on ecosystems (Yin *et al.*, 2016). They studied climate change patterns by examining vegetation cover and demonstrated the predictability of climate using the NDVI vegetation index. Other authors (Dastorani, 2021) explored vegetation changes and rainfall variations during the statistical period from 2001 to 2013 using satellite images. The outcomes highlighted the significance of both indicators at a 99% confidence level. The study showed a decline in the vegetation cover index within the lower class but an increasing trend in the middle and upper classes. In another study (Cui *et al.*, 2018), authors employed modeling and mapping techniques to analyze the relationship between spatial and temporal changes in vegetation and temperature and precipitation in the Yangtze basin from 2001 to 2013. They observed regions in the Yangtze river basin (YRB) with decreasing annual averages. Conversely, some areas within the basin displayed increasing trends during spring and summer, coupled with declining trends in autumn and winter. Overall, climatic factors emerged as the primary driver of NDVI changes in recent years. In another paper (Luan *et al.*, 2018), the spatial variations in vegetation within the Han River basin over the period 2000-2016 were analyzed using remote sensing data. The results indicated a noteworthy decrease of only 2.76% and an increase of 13.47%, with an overall increasing trend in NDVI for the region. Notably, the Shangzhou region showed the highest proportion of area with an increasing vegetation index trend at 11.31%.

In another study (Zhang D. *et al.*, 2020a), the stability and regression analysis methods were used to investigate the spatial changes in vegetation cover in the Marwarid River Delta area during the period from 2000 to 2015 on the basis of NDVI MODIS data. The findings revealed a consistent increase in vegetation cover during this time frame, suggesting a correlation between vegetation changes and human activities around the city. In a separate investigation (Kai-feng *et al.*, 2020), linear regression and Hurst's index were used to assess the temporal and mechanical changes in plant life within Three Rivers National Park. The results demonstrated that vegetation was on the rise in most areas of the park, with many displaying a positive trend of stability. In another study (Olafsson and Rousta, 2021), remote sensing was employed to explore the relationship between vegetation dynamics and weather patterns in Iceland from 2001 to 2019. The results indicated that vegetation in Iceland reaches its peak during the period from mid-July to late August, covering approximately 65% of the total area (66 858 km^2). In Rousta *et al.* (2022), ET, NDVI, and land surface temperature (LST) satellite images were utilized to investigate seasonal and annual vegetation dynamics and their connection to climatic factors in the Caspian Sea watersheds. The findings showed a positive and significant correlation between NDVI and ET in winter, NDVI and ET in spring, and NDVI and ET in summer, although the correlation became negative and significant between NDVI and LST during the summer season. This suggested that, in the summer, with higher-than-average rainfall, the influence of LST on plant growth becomes more pronounced. Other researchers (Yuan *et al.*, 2022) examined the temporal and spatial changes in vegetation in relation to climatic and human factors from 2000 to 2019 using the EVI vegetation index. The study highlighted the significant role of human factors in more than half of the green or brown areas, with changes being notable in only 9.9% of these areas. However, climate change emerged as the primary driver of EVI alterations and their mechanisms in mainland

China. Another study (Mahmood *et al.*, 2022) used MODIS data and precipitation data (PDIR Now) to assess the sustainability of spring vegetation changes in the watershed of northern Afghanistan from 2001 to 2020. The findings indicated 45.21% vegetation cover during the entire statistical period. Notably, the years 2001, 2008, and 2011 recorded the lowest vegetation levels at 9.9, 9.9, and 3.19%, respectively, coinciding with lower rainfall levels of 96.7, 133, and 117 mm. Conversely, the years 2003, 2009, and 2010 exhibited the most vegetation due to lower LST and higher precipitation, compared to the average period, resulting in wetter years.

The assessment of vegetation dynamics in the Yangtze river basin concerning climatic factors presents a complex challenge that necessitates a thorough evaluation. This basin holds immense significance within China, exerting a substantial influence on the country's economy, environment, and society. However, it grapples with numerous challenges, including climate change, alterations in land use and land cover, and human activities, all of which impact vegetation dynamics in the region. The crux of the issue lies in the limited understanding of how these factors affect vegetation cover within the basin and its sub-basins and how to effectively mitigate these effects. Hence, there arises a pressing need for a comprehensive assessment of vegetation dynamics in the Yangtze river basin and its correlation with climatic factors. This endeavor is essential to formulate effective strategies for ecosystem management and ensure sustainable development. Consequently, the primary objective of this study is to analyze the impact of climatic factors on vegetation dynamics within the Yangtze river basin during the period from 2001 to 2022, employing remote sensing data.

2. MATERIAL AND METHODS

2.1. Study area

The Yangtze river basin (YRB) stands as the largest river basin in China, and the Yangtze is one of the most significant rivers globally from socio-economic perspectives. Covering an extensive area of 1 808 500 km^2, it accounts for nearly a fifth of China's landmass and is inhabited by over 400 million people. Stretching over 6 300 km, it traverses more than halfway across China, ranking as the longest river in Asia and the third longest globally. The YRB is renowned for its rich biodiversity, housing over 10 000 species of plants and animals within its borders. Moreover, the YRB plays a pivotal and indispensable role in China's economy, serving as a crucial source of water for agriculture, hydroelectric power generation, and transportation. In this research, we have divided the YRB into three sub-basins: the upper sub-basin (UB), the middle sub-basin (MB), and the lower sub-basin (LB). The YRB plays a pivotal role in shaping food and agricultural production in China. Encompassing over 246 000 km^2, representing approximately 27% of China's total cultivated land area, the basin is characterized by its abundant water resources, rendering it highly conducive to rice cultivation. Notably, rice accounts for the largest proportion of cultivated lands within the basin, with approximately 70% of China's total rice output emanating from the YRB (Zhou *et al.*, 2024; Liang *et al.*, 2022) (Fig. 1). The average elevation of these three sub-basins is approximately: 3 493 m for UB, 900 m for MB, and 207 m for LB. Notably, the majority of the elevation is: 4 713, 31, and 26 m in: UB, MB, and LB, respectively. The annual precipitation in the three sub-basins is 9 74.6, 1 510.2, and 2 140.4 mm, respectively. Furthermore, the variations in LST for the three sub-basins are 14.9, 20.5, and 22.4°C, and the mean NDVI values are 0.41, 0.54, and 0.52, respectively (Table 1).

2.2. Data and methods

Remote sensing enables the collection of data from various points, objects, and environmental phenomena through different sensors, making it a fundamental branch of science (Gu *et al.*, 2007). In this research, the 16-day 250 m NDVI (MOD13Q1) and 8 day 1 km LST (MOD11A2) products from the MODIS sensor were analyzed, covering the statistical period from 2001 to 2022. These data were sourced from the United States Geological Survey website (https://lpdaacsvc.cr.usgs.gov/appeears/task/area). Additionally, monthly and annual CHIRPS rainfall data were downloaded (https://www.chc.ucsb.edu/data/chirps). All the calculations necessary to investigate the process of vegetation changes and their correlation with temperature and precipitation parameters were conducted using ArcGIS PRO and EXCEL software.

2.2.1. Normalized difference vegetation index (NDVI)

The most common and valuable index for assessing vegetation status is NDVI, which relies on measurements of the leaf area index (LAI) and production patterns (Dutta *et al.*, 2015; Dall'Olmo *et al.*, 2003). NDVI has been widely employed by scientists in various studies during the modern era (Martínez and Gilabert, 2009; Running *et al.*, 1995). The fundamental concept behind NDVI is rooted in the fact that the internal mesophyll of healthy green leaves strongly reflects near-infrared (NIR) radiation, while leaf chlorophyll and other pigments absorb a significant portion of red visible (RED) radiation (Broge and Leblanc, 2001). This relationship within the internal leaf structure is reversed in the case of unhealthy or water-stressed vegetation (Ghafarian Malamiri *et al.*, 2018). NDVI is calculated as:

$$NDVI = \frac{\mathrm{NIR}-\mathrm{RED}}{\mathrm{NIR}+\mathrm{RED}}.$$

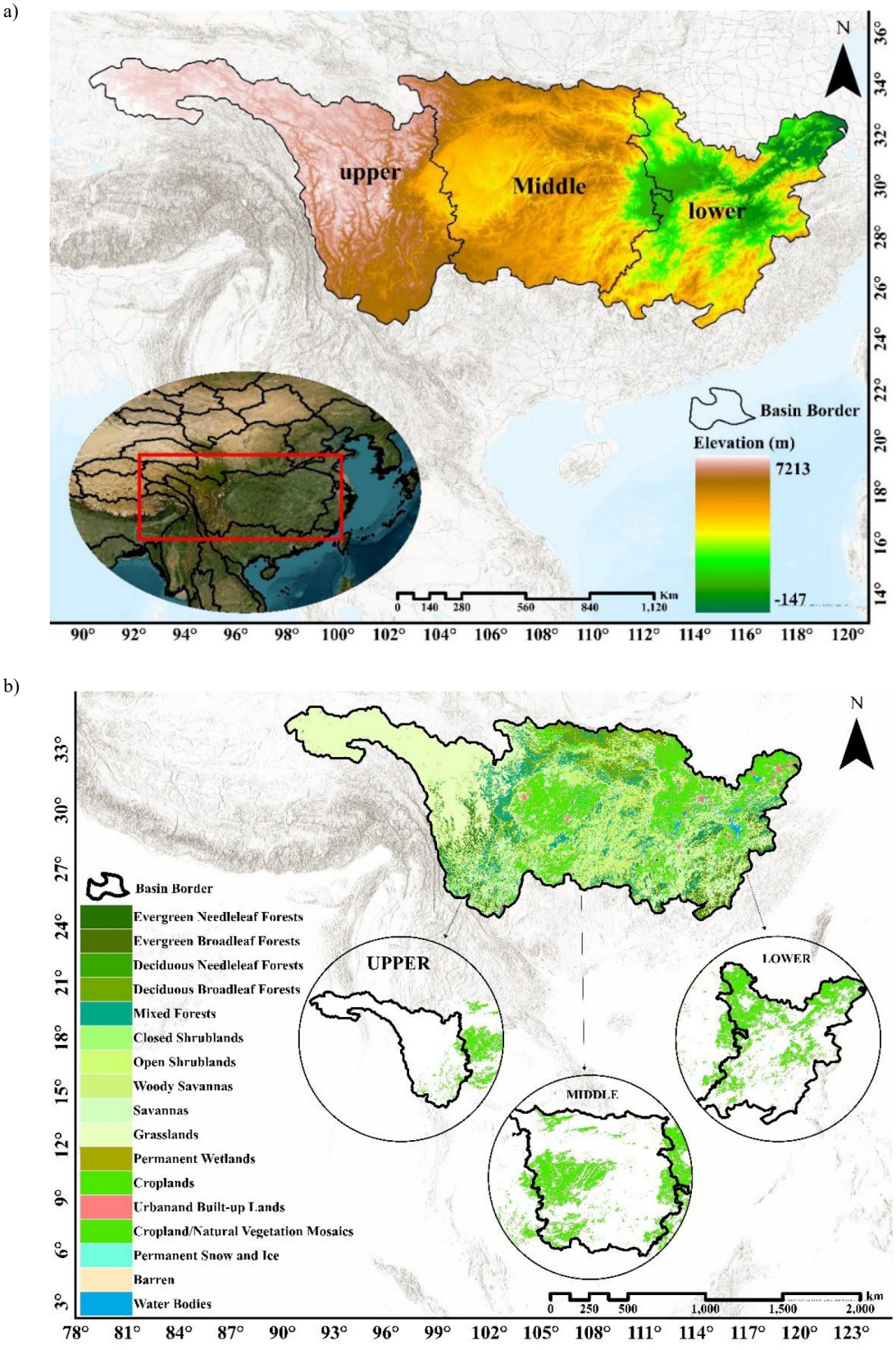

Fig. 1. Maps of a) geographical location of Yangtze River Basin with the elevation map, and b) YRB land cover map with the subpanels showing the locations of croplands for each Yangtze River subbasins separately (maps from MODIS MCD12Q1, 061, for 2018).

Table 1. Statistical features of the YRB divided into three sub-basins

Variable	Basin name	Area (km^2)	Min	Max	Mean	Majority
Elevation (m)	MB	694 293.8	11	5 411002	900.9	31
	UP	622 112.5	265	7 213	3 493.6	4 713
	LB	492 093.7	-147	2 064	207.3	26
Precip. (mm)	MB		651	2 536	1 510.2	1 567
	UP		258	2 555	974.7	1 082
	LB		953	3 836	2 140.4	2 265
LST (°C)	MB		-1	31	20	22
	UP		-11	33	14.4	11
	LB		11	28	21.9	22
NDVI	MB		-0.77	0.78	0.548	0.59
	UP		-0.13	0.84	0.417	0.53
	LB		-0.12	0.79	0.52	0.48

YRB – Yangtze river basin, MB – middle basin, UP – upper basin, LB – lower basin, LST – land surface temperature, NDVI – normalized difference vegetation index.

The NDVI index ranges from -1 to +1 (Rouse *et al.*, 1974). In this study, we obtained 506 images of Terra MODIS 16-day composite NDVI with a 250 m resolution (MOD13Q1, collection v006) from the Application for Extracting and Exploring Analysis Ready Samples (AppEEARS) software available at https://lpdaacsvc.cr.usgs.gov.appeears for the period 2001-2022 (Kalpoma *et al.*, 2019). NDVI values indicating vegetation range from 0.2 to 1, corresponding to areas with varying degrees of greenness or vegetation. It should be noted that NDVI values above 0.5 typically indicate a healthy and dense vegetation canopy, while values falling within the range of 0.2 to 0.5 are indicative of sparsely vegetated areas (Drori *et al.*, 2020). In the current study, the daily vegetation cover data were transformed into monthly, seasonal, and annual assessments and categorized into six classes (0.2-0.3, 0.3- 0.4, 0.4-0.5, 0.5-0.6, 0.6-0.7, and > 0.7). To calculate vegetation coverage (VegC), first the number of pixels in each NDVI class was calculated, then the number of pixels was multiplied by 250 m and finally converted to km^2.

2.2.2. Land surface temperature (LST)

Land surface temperature (LST) can be effectively derived using remote sensing tools (Şahin, 2012; Şahin *et al.*, 2013, 2014; Şenkal, 2010; Marj and Meijerink, 2011), which facilitate the examination of the radiative properties of the Earth's surface through an atmospheric window, without requiring a physical connection with the objects being investigated (Curran and Wardley, 1985). In this study, LST data were extracted from the Moderate Resolution Imaging Spectroradiometer (MODIS) radiometer onboard NASA-built satellites. It is important to note that the MODIS satellite has two primary sensors: Terra and Aqua (Wan, 1999; Wan *et al.*, 2002). In general, MODIS operates within the visible light and infrared spectrum, encompassing approximately 36 spectral bandwidths ranging from 0.4 to 14.4 μm wavelengths. For this research, to study the influence of temperature trends on vegetation, the 8 day LST data were transformed into monthly, seasonal, and annual datasets.

2.2.3. Precipitation (CHIRPS)

The CHIRP/S algorithm combines three main data sources: (a) Climate Hazards group Precipitation climatology (CHPclim), a global precipitation climatology at 0.05° latitude/longitude resolution, estimated for each month based on station data, averaged satellite observations, elevation, latitude, and longitude; (b) TIR-based satellite precipitation estimates (IRP); and (c) in-situ rain-gauge measurements. The CHPclim stands out from other precipitation climatologies because it utilizes long-term average satellite rainfall fields as a guide for deriving climatological surfaces, resulting in improved performance in mountainous regions like Ethiopia (Funk *et al.*, 2012; Peterson *et al.*, 2015). The CHIRPS product compiles over thirty years of global rainfall data, with a spatial resolution of approximately 0.05° worldwide. In the CHIRPS product, not only is satellite information utilized, but it is also verified by ground stations, making it a valuable resource for drought monitoring. CHIRPS data cover the region between 50°N and 50°S, spanning all longitudes, and has temporal coverage from January 1981 to the present day, offering daily, monthly, and seasonal values. These images were acquired monthly and annually during the statistical period from 2001 to 2022.

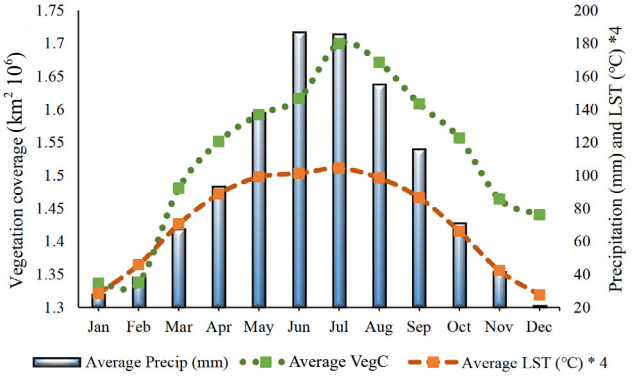

Fig. 2. Average values of precipitation, vegetation coverage (VegC), and land surface temperature (LST) in the Yangtze river basin (YRB) during the years 2001-2022 (to enhance visibility, the LST values have been multiplied by 4).

3. RESULTS

3.1. Vegetation coverage variations:

In Figure 2, changes in the average values of Vegetation Coverage (VegC), precipitation, and land surface temperature (LST) in the Yangtze river basin from 2001 to 2022 are presented. From this figure, it is evident that there is a correlation among all these parameters within the basin. Specifically, the highest VegC, precipitation, and LST occur during June and July, while the lowest values are observed in December, January, February, and November. This observation underscores the interconnectedness between precipitation and LST in the basin, which collectively influenced the VegC dynamics in the area throughout the study period (2001-2022).

Figure 3 shows the changes in VegC during 2001-2022 in the YRB in the form of a yearly averaged time series. It is evident that there is a notable and statistically significant

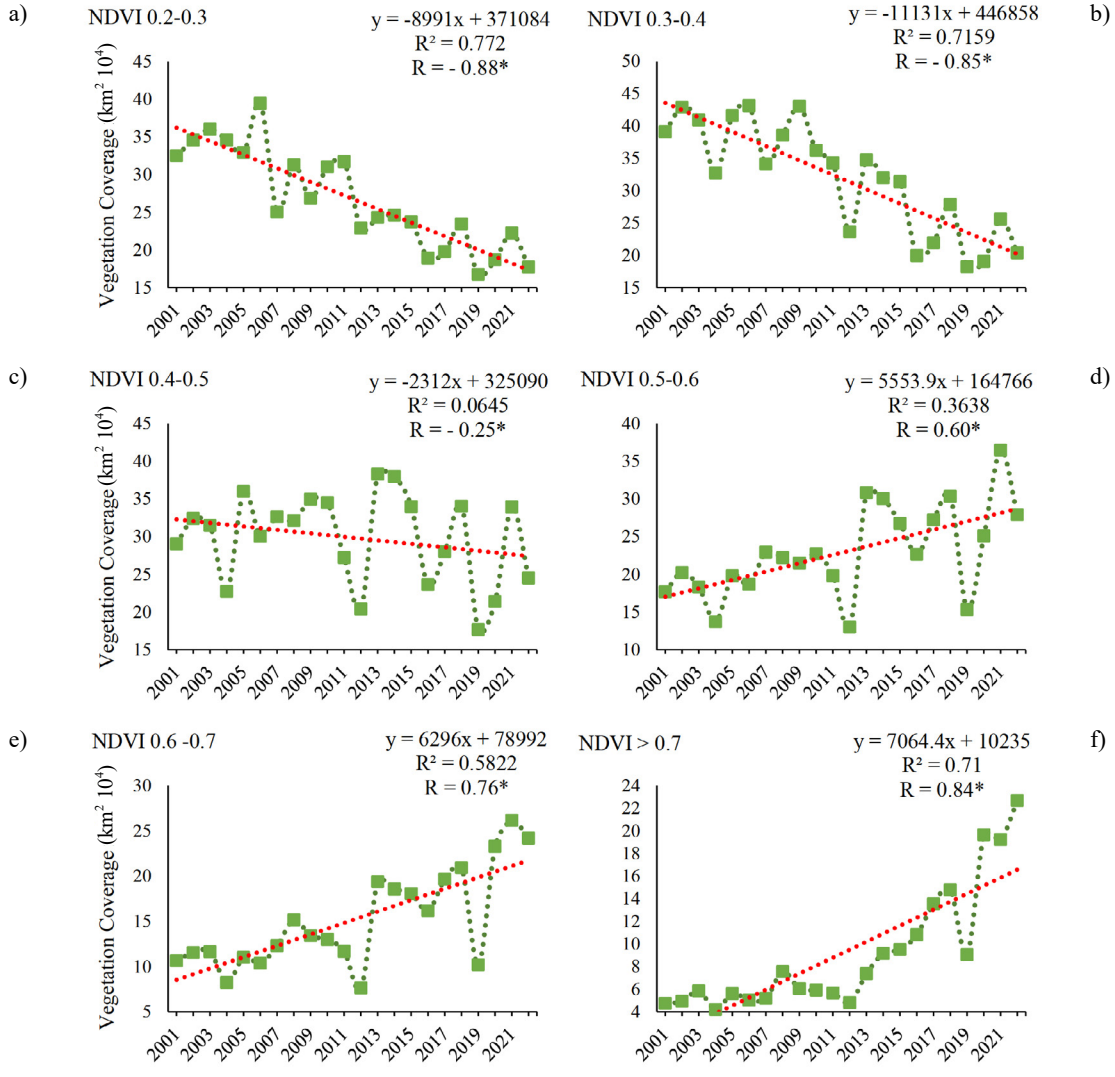

Fig. 3. Yearly averaged time series of changes in VegC (km² 10^4) separated into different categories of NDVI in the YRB during 2001-2022, namely a) 0.2-0.3, b) 0.3-0.4, c) 0.4-0.5, d) 0.5-0.6, e) 0.6-0.7, and f) > 0.7. (*Denotes a correlation significant at p-value = 0.05).

declining trend in VegC for categories 0.2-0.4, with correlation coefficients R = -0.88 and -0.85 (at p-value = 0.05), respectively. Additionally, there is a decreasing trend, albeit not statistically significant, in VegC for category 0.4-0.5 in the study area during this time frame. Conversely, the figure demonstrates a clear and statistically significant upward trend in VegC for categories > 0.5 across the entire basin during 2001-2022, with R = 0.6, 0.76, and 0.84 (at p-value = 0.05), respectively. As a result, there was a declining trend in the area covered by more sparse vegetation and a concurrent increasing trend in the area covered by denser vegetation within the YRB throughout the study period.

3.2. Anomaly of VegC

Figure 4 presents the time series of anomalies in yearly vegetation coverage (VegC), precipitation, and land surface temperature (LST) within the Yangtze river basin (YRB) for the years 2001-2022. The figure suggests a stronger correlation between VegC and LST, compared to precipitation. It is noticeable that years with the lowest VegC correspond to the lowest LST (*e.g.*, 2005 and 2012), while years with the highest VegC coincide with normal or above-normal LST (*e.g.*, 2013 and 2021). However, there are exceptions, such as 2004 and 2019, which exhibit high and low VegC values during 2001-2022. For these two years (2004 and 2019), it appears that other factors influenced VegC in the area, and these factors may not have had a uniform impact across all regions of the YRB, potentially exerting a negative effect on VegC in some areas and a positive effect in others.

Figure 5 illustrates the time series of annual changes in VegC across different seasons, while Figure 6 shows the anomaly of annual changes in VegC. The largest VegC area is observed during the summer season, while the smallest is noted during the winter season. Winter and spring in 2012 recorded 1 131 ,793 km^2 and 1 501 190 km^2 of VegC, respectively, with summer in 2020 reaching 1 563 193 km^2 and fall in 2001 at 1 376 283 km^2, which is the lowest. Winter and summer in 2021, spring in 2011, and fall in 2012 all exceeded the normal levels. Conversely, winter and spring in 2012, summer in 2020, and fall in 2001 all fell below normal levels.

In Table 2, the correlation between yearly and seasonal vegetation with LST and precipitation in the YRB is presented. An upward trend and a significant increase in winter and summer VegC with yearly VegC (R = 0.88 and R = 0.42, at p-value = 0.05) and a significant positive correlation between LST and yearly VegC (R = 0.75, at p-value = 0.05) were observed.

Table 3 shows the correlation between monthly VegC and LST and precipitation. Significant positive correlations between VegC and LST in several months (Jan, Feb, Mar,

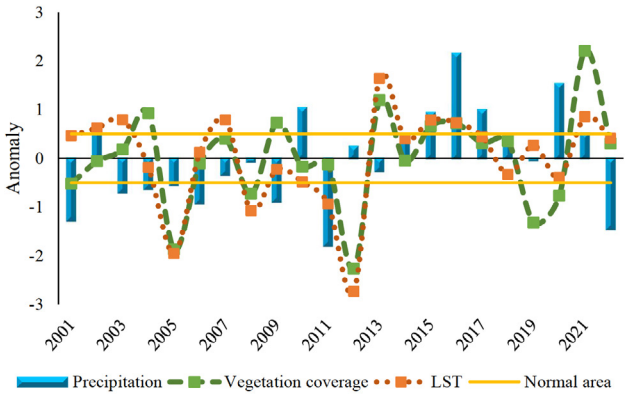

Fig. 4. Anomaly of yearly VegC, precipitation, and LST in the YRB during 2001-2022.

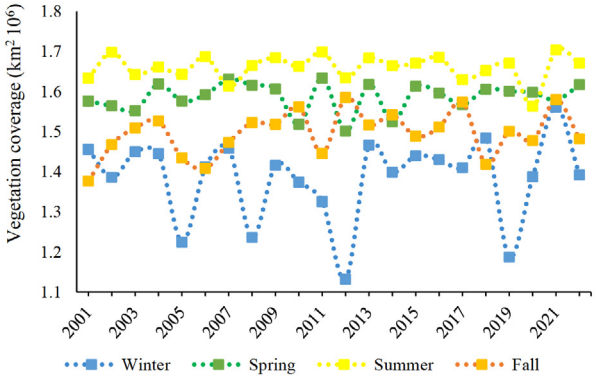

Fig. 5. Yearly average seasonal changes in VegC in the YRB during 2001-2022.

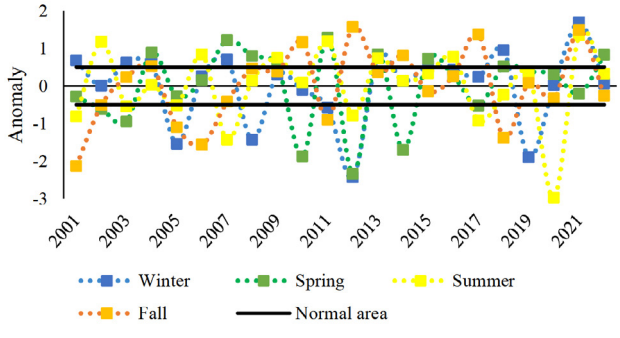

Fig. 6. Anomaly of seasonal VegC in the YRB during 2001-2022.

Table 2. Correlation coefficients (R) between yearly VegC, seasonal and yearly precipitation, and LST in YRB during 2001-2022

Correlation	Winter	Spring	Summer	Fall	Yearly VegC
Yearly VegC	0.88*	0.38	0.42*	0.18	1
LST	0.75	0.31	0.23	-0.04	0.75*
Precipitation	0.08	-0.32	-0.20	0.43	0.08

LST – land surface temperature, YRB – Yangtze river basin.

Table 3. Correlation coefficients (R) between monthly VegC and monthly precipitation and LST in YRB during 2001-2022

Correlation VegC	LST	Precipitation
Jan	0.59*	-0.04
Feb	0.56*	-0.14
Mar	0.47*	-0.18
Apr	0.04	-0.29
May	0.58*	0.02
Jun	0.56*	-0.14
Jul	0.73*	-0.53*
Aug	0.47*	-0.37
Sep	0.42*	-0.23
Oct	0.31	0.09
Nov	0.21	0.11
Dec	0.28	-0.28

Explanations as in Table 2.

May, Jun, Jul, Aug, Sep) and a negative correlation between VegC and July precipitation (r = 0.53, p-value = 0.05) were observed.

Table 4 displays the monthly VegC in the YRB. The most significant decreases in VegC occurred in Jan 2005 and 2008, Feb 2012 and 2019, Mar 2010, Apr 2002, May 2012, Jun 2017, Aug 2007, Sep 2020, Nov 2001, 2006, and 2020, and Dec 2019. In contrast, the highest increases in VegC were observed in Mar 2007 and 2018, May 2018, Jun 2022, Jul 2006, 2021, and 2022, Aug 2002, 2011, and 2020, Oct 2020, and Dec 2021. Figure 7 highlights the four instances with the most significant reductions in VegC in the YRB. According to the figure, the most substantial VegC reduction occurred in Apr 2002 in MB and LB, in Mar 2010 in MB and UB, in Dec 2019 in UB and MB, and in Sep 2020 in MB. Based on the histograms of each image, the highest amount of VegC falls within the 0.2 to 0.5 classes, representing weak to medium vegetation. On the other hand, Fig. 8 illustrates the highest monthly VegC increases in August, October, and July. In the images, the north of UB exhibits the lowest vegetation. In October 2020, due to the autumn season and a decrease in VegC density in MB and LB, the density of dense vegetation also decreased. The histograms of each image show the highest amount of VegC in the upper 0.5 layers, representing dense vegetation.

3.3. Vegetation variations in three sub-basins of YRB

Figure 9 illustrates changes in the total area of VegC in UB, MB, and LB. MB consistently has the largest area of VegC. The lowest VegC values were recorded in UB in 2008 (520 518.8 km^2), MB in 2001 (689 353.8 km^2), and LB in 2005 (480 419.7 km^2). Conversely, the largest VegC areas in all three basins occurred in 2021, totaling 581 461.8, 743 734.2, and 587 089.5 km^2, respectively. A significant upward trend and a substantial increase in VegC (at p-value = 0.01) observed in all three basins between 2001 and 2022 was observed (Table 5).

3.3.1. Anomaly of VegC in UB, MB, and LB

Figure 10 presents the anomaly of the annual VegC time series in UB, MB, and LB. The figure shows a strong correlation between VegC and LST in all three basins. For instance, in 2011, LST and VegC were within the normal range in all three basins, despite below-normal precipitation. In 2021, when there was the largest area of VegC in all three basins, the conditions varied. In UB, LST and precipitation are within the normal range, in MB, LST is within the normal range and precipitation is above normal, and in LB, precipitation is within the normal range, but LST is above normal. However, it is important to note that this pattern is not consistent across all years and basins. For instance, in UB in 2001, despite LST and precipitation being in the normal range, VegC is lower than normal. In MB in 2006, although LST was higher than normal, VegC was lower than normal. In LB in 2008, despite higher than normal LST and normal precipitation, VegC decreased. Therefore, it can be concluded that the relationship between the increase in VegC, LST, and precipitation (especially LST) cannot be generalized to the entire basin at all times.

Table 6 displays the correlation between VegC, precipitation, and LST in all three basins. It indicates an upward trend and a significant increase in VegC correlated with LST. Figure 11 illustrates the distribution of annual VegC with LST and precipitation in UB, MB, and LB. The results presented in this figure indicate an overall upward trend in annual VegC across all three basins, which is particularly prominent in LB and significantly associated with an increase in LST (at p-value = 0.05).

4. DISCUSSION

Vegetation coverage (VegC) is frequently used to assess natural habitats, playing a key role in determining the impact of changes in farmland on the surrounding environment (Zhang Y. *et al.*, 2020c; Gou *et al.*, 2024). In this research, the vegetation changes and the impact of temperature and

Table 4. Anomaly of monthly vegetation coverage (VegC) in YRB during 2001-2022

Year	Vegetation coverage (VegC) anomaly											
	Jan	Feb	Mar	Apr	May	Jun	Jul	Aug	Sep	Oct	Nov	Dec
2001	0.54	0.79	-0.04	-0.61	-1.08	0.92	0.57	-1.29	-0.42	0.11	-2.09	-0.92
2002	-0.14	-0.40	1.11	-4.03	0.29	0.99	0.33	1.37	0.42	-0.44	0.35	-0.19
2003	0.43	0.27	0.74	0.35	-1.86	-0.43	-0.13	-0.78	-0.13	1.10	-0.16	0.17
2004	0.58	0.96	0.72	0.50	0.31	0.49	-0.01	-1.34	0.74	-0.08	0.47	-0.53
2005	-2.50	0.08	-0.37	-0.10	-0.86	0.49	-1.56	-0.01	0.05	-1.16	-0.81	0.45
2006	0.03	0.21	-0.20	-0.02	-0.63	0.87	1.26	0.19	0.32	-0.61	-2.08	0.64
2007	0.66	0.42	1.33	0.57	0.32	0.71	-0.21	-2.01	-0.40	-1.39	0.00	0.10
2008	-2.32	-0.02	-0.23	0.19	0.54	0.84	-0.44	-0.69	0.69	0.07	0.68	0.42
2009	0.96	-0.51	-1.01	0.72	0.78	-0.77	-1.55	1.04	0.86	0.31	0.08	0.64
2010	-0.73	0.89	-2.64	0.41	-0.32	-1.32	-0.98	0.38	0.27	0.87	0.60	0.73
2011	-0.80	0.26	-0.26	0.44	1.05	0.82	1.02	1.35	0.18	-0.43	-0.09	-0.97
2012	-1.04	-2.50	-0.83	0.18	-2.07	-0.98	-1.56	0.66	-0.60	1.12	0.76	-1.16
2013	0.02	1.11	0.05	-0.84	0.83	1.00	0.48	-0.74	1.00	-1.13	0.92	1.05
2014	0.27	-0.47	-0.62	0.15	-1.35	-1.66	-0.97	-0.89	0.99	0.36	0.36	1.14
2015	1.01	-0.91	1.08	0.22	0.29	0.39	0.90	-0.89	0.48	0.35	-0.47	0.34
2016	0.70	0.74	-0.51	-0.05	1.07	-0.05	0.30	0.91	0.24	-1.93	1.13	-0.56
2017	1.05	-1.05	0.70	-0.04	1.04	-2.08	0.48	0.10	-1.23	0.71	0.69	0.44
2018	0.23	0.96	1.31	-0.39	1.31	-0.71	-0.55	0.71	-0.41	0.70	0.34	-1.59
2019	-0.10	-2.42	0.66	0.63	1.11	-1.32	0.67	0.14	0.02	1.11	0.15	-2.60
2020	0.51	0.39	-1.42	0.09	0.01	0.03	-1.21	1.46	-3.49	1.93	-2.20	0.03
2021	1.23	0.46	-0.64	0.98	0.12	0.40	1.55	-0.64	1.19	0.00	1.37	1.76
2022	-0.60	0.75	1.05	0.65	-0.90	1.37	1.59	0.97	-0.77	-1.57	0.00	0.59

YRB – Yangtze river basin.

precipitation variations on these changes were investigated using remote sensing data over the past 22 years (2001-2022) in the Yangtze river basin. The analysis of vegetation coverage in the Yangtze river basin reveals several trends. The highest values are observed in June and July, while the lowest values occur in December, January, February, and November. This pattern underscores the significant influence of precipitation and temperature on vegetation in the region. Furthermore, a decreasing trend in the area covered by sparse vegetation (0.2-0.5) and an increasing trend in denser vegetation areas (above 0.5) were identified during the study period. While vegetation coverage exhibits a stronger correlation with temperature than with precipitation, it is important to note that this relationship cannot be generalized to the entire basin at all times. Seasonal variations reveal that vegetation, temperature, and precipitation interact in complex ways, likely influenced by such factors as climate, topography, and human activities. Based on our analysis of annual maps, we found that the middle basin (MB) consistently had the largest vegetation area, while the lowest area was recorded in the upper basin (UB) in 2008, the middle basin (MB) in 2001, and the lower basin (LB) in 2005. The largest vegetation area in all three basins was observed in 2021, highlighting the spatial variability in environmental conditions and factors affecting vegetation across the Yangtze river basin.

In summary, our findings indicate an overall upward trend and a significant increase in vegetation in all three basins during the 2001-2022 period, aligning with previous studies (Qu *et al.*, 2020; Zhang Y.-X. *et al.*, 2020b; Cui *et al.*, 2019; Liu *et al.*, 2022). The observed decline in scattered vegetation cover and the rise in dense vegetation align with the global trends of increased vegetation in response to climate change (Xu *et al.*, 2013; Zhu *et al.*, 2016). The stronger correlation between vegetation cover and land surface temperature, compared to precipitation, underscores the pivotal role of temperature in driving vegetation changes in the Yangtze river basin, in line with the concept of thermal adaptation, which underscores plant sensitivity to temperature fluctuations (Wu *et al.*, 2011).

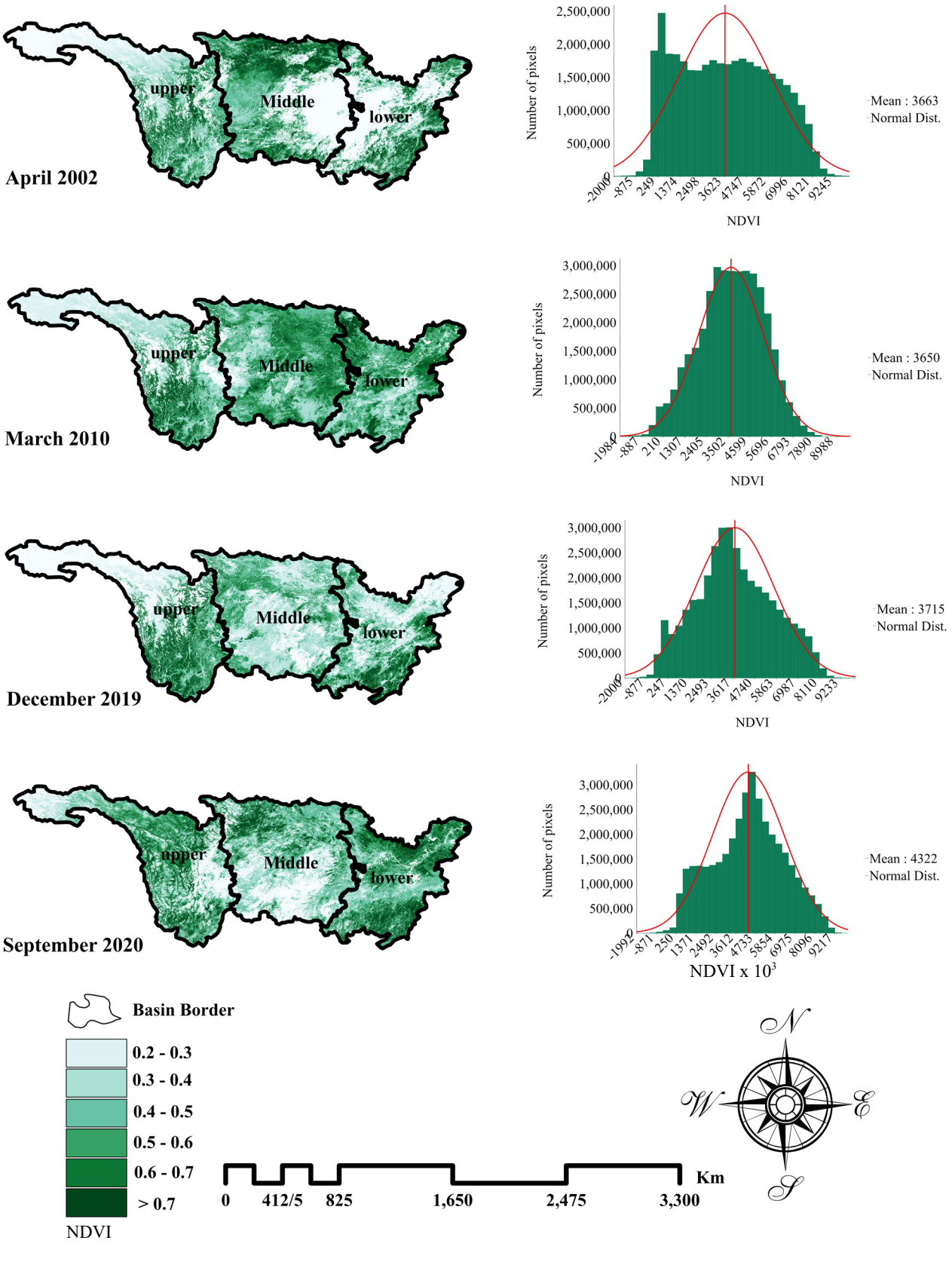

Fig. 7. Maps presenting the months with highest VegC reduction in the YRB during 2001-2022.

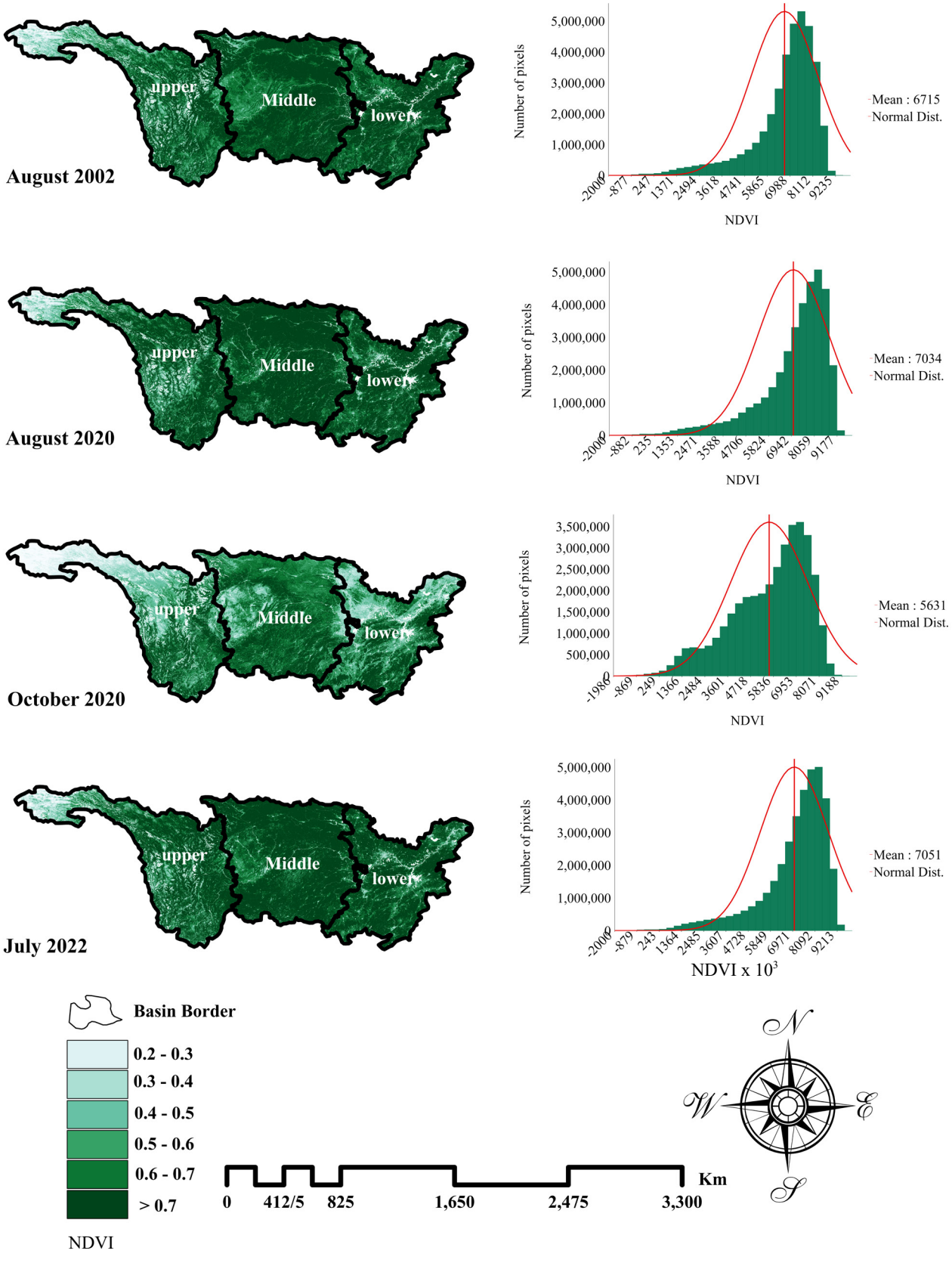

Fig. 8. Maps presenting the highest increase in monthly VegC in the YRB during 2001-2022.

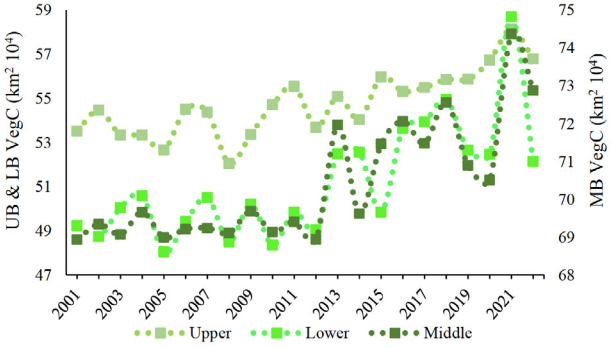

Fig. 9. Time series of yearly averages of VegC in UB, MB, and LB in the YRB.

Table 5. Trends in annual VegC changes in UB, MB, and LB in YRB

Yangtze river basin	UB	MB	LB
Year	0.651*	0.593*	0.498*

Explanations as in Table 1. *Denotes a correlation significant at p-value = 0.01.

After analyzing vegetation cover, precipitation, and land surface temperature in the Yangtze river basin (YRB) for the 2001-2022 period, a complex interplay between these parameters was identified. Notably, temperature exerts a more pronounced influence on vegetation changes than precipitation, consistent with findings from previous studies (Zhang and Jin, 2021; Qu *et al.*, 2018). However, it is essential to acknowledge that, in certain years, this correlation appears to be absent, suggesting the involvement of other influential factors in driving vegetation changes. These additional factors may encompass disturbances, such as wildfires or localized weather events, each of which can have varying impacts across the watershed. Understanding these nuances in vegetation dynamics within the Yangtze river basin holds significant importance for effective land management and conservation strategies. This study contributes to the existing knowledge base by offering a comprehensive analysis that sheds light on these intricate relationships within the YRB. The observed trends in vegetation underscore the urgency of implementing sustainable land use practices and ecosystem protection measures in the region. These measures could encompass initiatives related to reforestation, forestry management, and water resource management, all of which can support the growth and preservation of vegetation in the YRB. Furthermore, further research is warranted to fully grasp the factors driving vegetation changes in the region, including the roles of human activities, climate shifts, and natural disturbances.

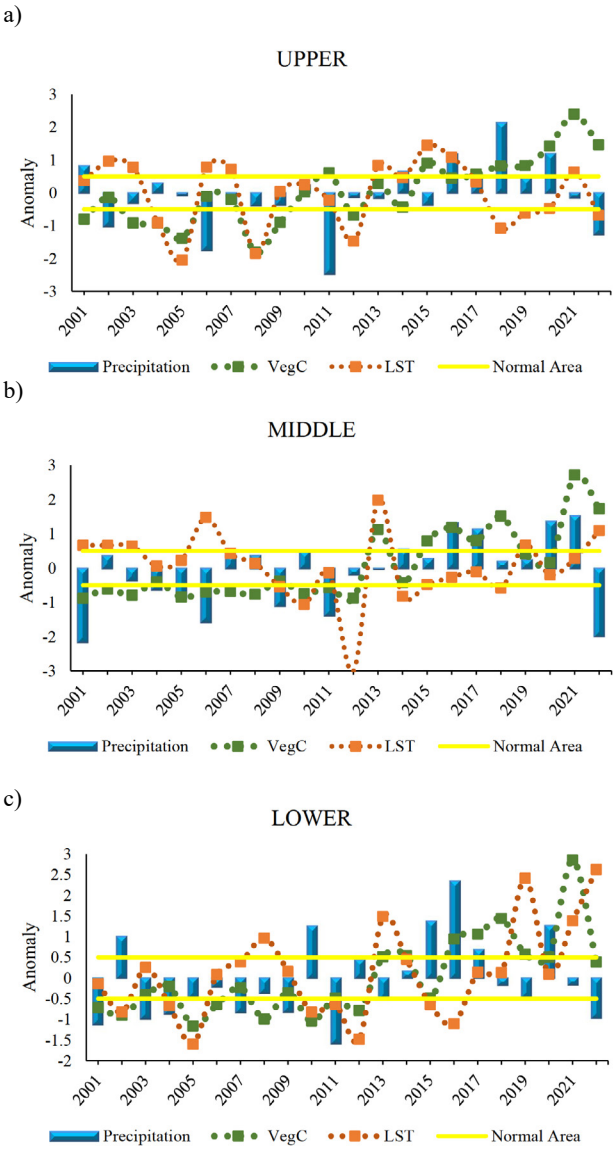

Fig. 10. Anomaly of yearly VegC, precipitation, and LST in: a) UB, b) MB, and c) LB during 2001-2022.

Table 6. Correlation between VegC with LST and precipitation in UB, MB, and LB during 2001-2022

Correlation	LST	Precipitation
VegC Upper	0.165	0.52
VegC Middle	0.004	0.255
VegC Lower	0.377*	0.108

Explanations as in Table 1. *Denotes a correlation significant at p-value = 0.05.

In summary, these findings contribute significantly to our comprehension of ecosystem dynamics in the Yangtze river basin and highlight the necessity of informed sustainable approaches to safeguard its natural resources.

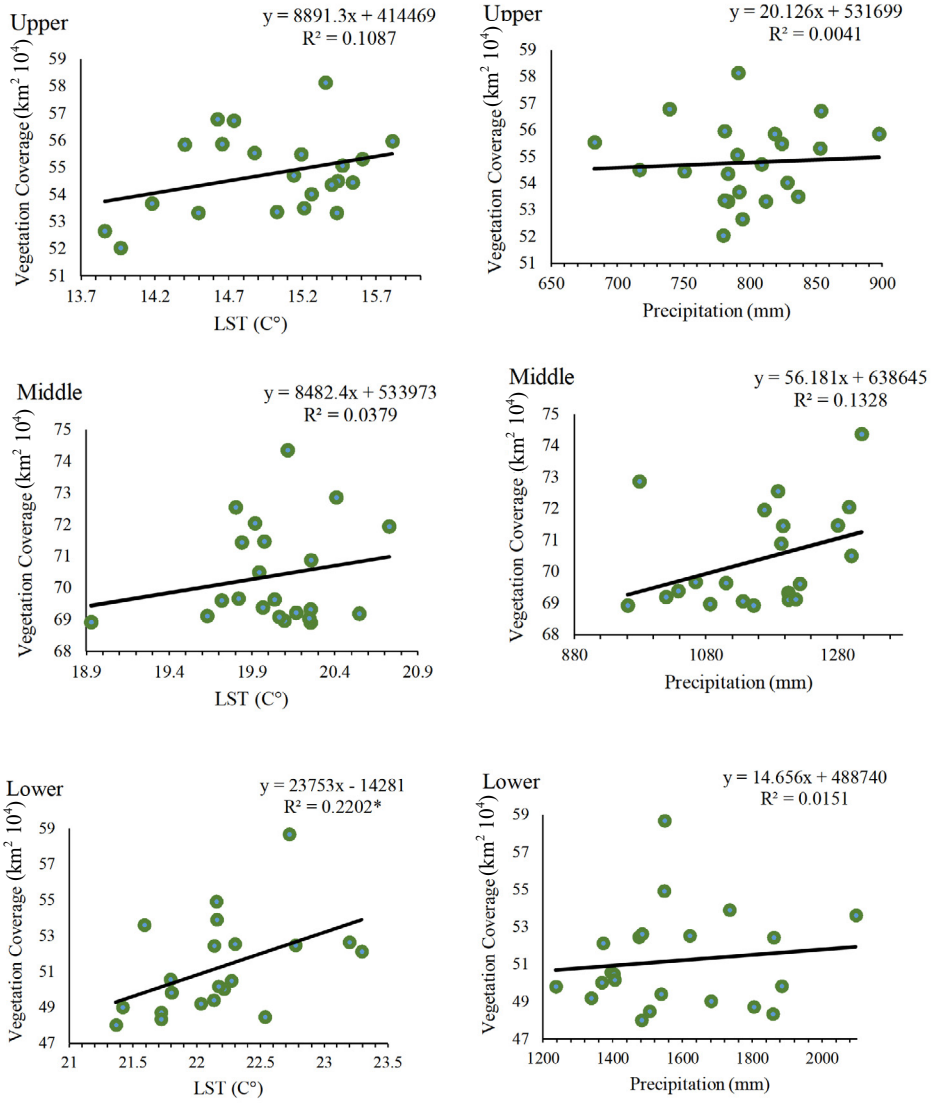

Fig. 11. Distribution of annual VegC (km^2) with precipitation and LST in UB, MB, and LB in the YRB.

5. CONCLUSIONS

In this study, the dynamics of vegetation cover and its sensitivity to temperature and precipitation changes in the Yangtze river basin were investigated. The basin was divided into three sub-basins: the upper basin (UB), middle basin (MB), and lower basin (LB). By analyzing a 22-year time series (2001-2022) of the normalized vegetation difference index (NDVI), precipitation, and LST from remote sensing data, changes on an annual, seasonal, and monthly basis were analyzed. The relationship between NDVI changes and precipitation as well as temperature was evaluated using Kendall's correlation. The Yangtze river basin exhibited the highest NDVI values in July and August, while the lowest values were observed in February and January. Similarly, peak precipitation occurred during the summer months of June, July, and August, with the highest land surface temperatures recorded in May, June, July, and August. Regarding vegetation coverage (VegC), the most extensive areas were seen in winter and spring 2012 (1 131 793 and 1 501 190 km^2, respectively), summer 2020 (1 563 193 km^2), and fall 2001 (1 376 283 km^2). Conversely, the smallest VegC areas were recorded in winter and summer 2021 (1 561 014 and 1 703 521 km^2, respectively). In terms of NDVI classes, we observed a declining trend with a significant decrease (p-value = 0.05) in the 0.2-0.5 range. Conversely, classes 0.5-0.7 and higher exhibited an upward trend with a significant increase (p-value = 0.05). This suggests a decrease in the weak and moderate NDVI and an increase in the high and very high NDVI across the entire Yangtze river basin. Furthermore, the middle basin (MB) displayed the most substantial increase in the NDVI area,

while the upper basin (UB) in 2008, middle basin (MB) in 2001, and lower basin (LB) in 2005 recorded the lowest values.

In summary, the overall increase in VegC throughout the Yangtze river basin demonstrated a stronger correlation with temperature than with precipitation. However, to gain a more comprehensive understanding of these results, it is imperative to consider additional factors, such as sunlight, soil moisture, and other variables that may influence the ecosystem. Nonetheless, these findings provide valuable insights for future research and management strategies aimed at preserving and enhancing the ecological health of the Yangtze river basin.

Conflicts of Interest: The Authors do not declare any conflict of interest.

6. REFERENCES

Angelini, I.M., Garstang, M., Davis, R.E., Hayden, B., Fitzjarrald, D.R., Legates, D.R., *et al*., 2011. On the coupling between vegetation and the atmosphere. Theoretical Appl. Climatol. 105, 243-261. https://doi.org/10.1007/s00704-010-0377-5

Aronoff, S., 2004. Remote sensing for GIS managers. Environmental Systems Research, University of Minnesota, USA.

Broge, N.H., Leblanc, E., 2001. Comparing prediction power and stability of broadband and hyperspectral vegetation indices for estimation of green leaf area index and canopy chlorophyll density. Remote Sensing Environ. 76, 156-172. https://doi.org/10.1016/S0034-4257(00)00197-8

Chen, X., Xie, D., Zhang, Z., Sharma, R.P., Chen, Q., Liu, Q., *et al*., 2023. Compatible biomass model with measurement error using airborne LiDAR data. Remote Sensing 15, 3546. https://doi.org/10.3390/rs15143546

Cheng, P., Wu, L., Zhang, H., Zhou, J., 2024. Inclusion of root water absorption and reinforcement in upper bound limit stability analysis of vegetated slopes. Computers Geotechnics 169, 106227. https://doi.org/10.1016/j.compgeo.2024.106227

Cui, L., Wang, L., Qu, S., Singh, R.P., Lai, Z., Yao, R., 2019. Spatiotemporal extremes of temperature and precipitation during 1960-2015 in the Yangtze River Basin (China) and impacts on vegetation dynamics. Theoretical Appl. Climatol. 136, 675-692. https://doi.org/10.1007/s00704-018-2519-0

Cui, L., Wang, L., Singh, R.P., Lai, Z., Jiang, L., Yao, R., 2018. Association analysis between spatiotemporal variation of vegetation greenness and precipitation/temperature in the Yangtze River Basin (China). Environ. Sci. Pollution Res. 25, 21867-21878. https://doi.org/10.1007/s11356-018-2340-4

Curran, P., Wardley, N., 1985. Remote sensing in secondary school geography: the place of Landsat MSS. Geography 70, 237-240.

Dall'olmo, G., Gitelson, A.A., Rundquist, D.C., 2003. Towards a unified approach for remote estimation of chlorophyll-a in both terrestrial vegetation and turbid productive waters. Geophys. Res. Letters 30. https://doi.org/10.1029/2003GL018065

Dastorani, M., 2021. Assessing the Vulnerability of the Land Using the IDI Combination Model in Arid and Semi arid Regions (Khorasan Razavi). J. Arid Regions Geographics Studies 12, 78-90.

Drori, R., Dan, H., Sprintsin, M., Sheffer, E., 2020. Precipitation-sensitive dynamic threshold: A new and simple method to detect and monitor forest and woody vegetation cover in sub-humid to arid areas. Remote Sensing 12, 1231. https://doi.org/10.3390/rs12081231

Dutta, D., Kundu, A., Patel, N., Saha, S., Siddiqui, A., 2015. Assessment of agricultural drought in Rajasthan (India) using remote sensing derived Vegetation Condition Index (VCI) and Standardized Precipitation Index (SPI). Egyptian J. Remote Sensing Space Sci. 18, 53-63. https://doi.org/10.1016/j.ejrs.2015.03.006

Funk, C., Michaelsen, J., Marshall, M.T., 2012. Mapping recent decadal climate variations in precipitation and temperature across eastern Africa. Remote Sensing Drought: Innovative Monitoring Approaches 331, 331-355.

Ghafarian Malamiri, H.R., Rousta, I., Olafsson, H., Zare, H., Zhang, H., 2018. Gap-filling of MODIS time series land surface temperature (LST) products using singular spectrum analysis (SSA). Atmosphere 9, 334. https://doi.org/10.3390/atmos9090334

Gou, Y., Jin, Z., Kou, P., Tao, Y., Xu, Q., Zhu, W., *et al*., 2024. Mechanisms of climate change impacts on vegetation and prediction of changes on the Loess Plateau, China. Environ. Earth Sci. 83, 234. https://doi.org/10.1007/s12665-024-11559-5

Gu, X., Li, Y., Zuo, X., Bu, J., Yang, F., Yang, X., *et al*., 2024. Image compression-based DS-InSAR method for landslide identification and monitoring of alpine canyon region: a case study of Ahai Reservoir area in Jinsha River Basin. Landslides 1-17. https://doi.org/10.1007/s10346-024-02299-5

Gu, Y., Brown, J.F., Verdin, J.P., Wardlow, B., 2007. A five-year analysis of MODIS NDVI and NDWI for grassland drought assessment over the central Great Plains of the United States. Geophysical Res. Letters 34. https://doi.org/10.1029/2006GL029127

Guo, L., Wu, S., Zhao, D., Yin, Y., Leng, G., Zhang, Q., 2014. NDVI-based vegetation change in Inner Mongolia from 1982 to 2006 and its relationship to climate at the biome scale. Advances in Meteorol. 2014, 1-12. https://doi.org/10.1155/2014/692068

Hu, Y., Dao, R., Hu, Y., 2019. Vegetation change and driving factors: Contribution analysis in the loess plateau of China during 2000-2015. Sustainability 11, 1320. https://doi.org/10.3390/su11051320

Kafarski, M., Majcher, J., Wilczek, A., Szypłowska, A., Lewandowski, A., Zackiewicz, A., *et al*., 2019. Penetration depth of a soil moisture profile probe working in time-domain transmission mode. Sensors 19, 5485. https://doi.org/10.3390/s19245485

Kai-Feng, P., Wei-Guo, J., Peng, H., Chen-Xi, S., Xiang, Z., Ru-Lin, X., 2020. Spatiotemporal variation of vegetation coverage and its affecting factors in the Three river source National Park. Chinese J. Ecol. 39, 3388-3396.

Kalpoma, K.A., Chowdhury, A., Arony, N.N., Nowshin, M., Kudoh, J.-I., 2019. New modis vegetation index for Boro rice model using 3d plot and K-NN: Bangladesh Haor region perspective. IGARSS 2019-2019 IEEE Int. Geosci. Remote Sensing Symp., IEEE 7322-7325. https://doi.org/10.1109/IGARSS.2019.8898950

Katiraie Boroujerdy, P.S., 2016. Comparison of high-resolution gridded monthly satellite and ground-based precipitation data over Iran. Iranian J. Geophys. 7, 149-160.

Kundu, A., Dwivedi, S., Dutta, D., 2016. Monitoring the vegetation health over India during contrasting monsoon years using satellite remote sensing indices. Arabian J. Geosci. 9, 1-15. https://doi.org/10.1007/s12517-015-2185-9

Li, J., Zhao, Y., Chen, D., Zhao, P., Zhang, C., Wang, Y., 2024. The Quantitative Role of Moisture and Vertical Motion in Shaping Summer Heavy Rainfall over North China under Two Distinct Large-Scale Weather Patterns. J. Climate 37, 2655-2672. https://doi.org/10.1175/JCLI-D-22-0850.1

Liang, H., Meng, Y., Ishii, K., 2022. The effect of agricultural greenhouse gas emissions reduction policies: evidence from the middle and lower basin of Yangtze River, China. Discover Sustain. 3, 43. https://doi.org/10.1007/s43621-022-00107-5

Liu, C., Shan, Y., He, L., Li, F., Liu, X., Nepf, H., 2024. Plant morphology impacts bedload sediment transport. Geophys. Res. Letters 51, e2024GL108800. https://doi.org/10.1029/2024GL108800

Liu, J., Liu, S., Tang, X., Ding, Z., Ma, M., Yu, P., 2022. The response of land surface temperature changes to the vegetation dynamics in the Yangtze River Basin. Remote Sensing 14, 5093. https://doi.org/10.3390/rs14205093

Luan, J., Liu, D., Zhang, L., Huang, Q., Feng, J., Lin, M., *et al*., 2018. Analysis of the spatial-temporal change of the vegetation index in the upper reach of Han River Basin in 2000-2016. Proc. IAHS 379, 287-292. https://doi.org/10.5194/piahs-379-287-2018

Luo, Q., Bai, X., Zhao, C., Luo, G., Li, C., Ran, C., *et al*., 2024. Unexpected response of terrestrial carbon sink to rural depopulation in China. Sci. Total Environ. 174595. https://doi.org/10.1016/j.scitotenv.2024.174595

Mahmood, S.A.R., Rousta, I., Mazidi, A., 2022. Investigating the sustainability of vegetation change trends using remote sensing (Case Study: Northern River Basin of Afghanistan). Geography Environ. Sustain. 12, 17-35.

Majcher, J., Kafarski, M., Wilczek, A., Szypłowska, A., Lewandowski, A., Woszczyk, A., *et al*., 2021. Application of a dagger probe for soil dielectric permittivity measurement by TDR. Measurement 178, 109368. https://doi.org/10.1016/j.measurement.2021.109368

Marj, A.F., Meijerink, A.M., 2011. Agricultural drought forecasting using satellite images, climate indices and artificial neural network. Int. J. Remote Sensing 32, 9707-9719. https://doi.org/10.1080/01431161.2011.575896

Martínez, B., Gilabert, M.A., 2009. Vegetation dynamics from NDVI time series analysis using the wavelet transform. Remote Sensing Environ. 113, 1823-1842. https://doi.org/10.1016/j.rse.2009.04.016

Olafsson, H., Rousta, I., 2021. Influence of atmospheric patterns and North Atlantic Oscillation (NAO) on vegetation dynamics in Iceland using Remote Sensing. Eur. J. Remote Sensing 54, 351-363. https://doi.org/10.1080/22797254.2021.1931462

Peterson, P., Funk, C.C., Landsfeld, M.F., Pedreros, D.H., Shukla, S., Husak, G.J., *et al*., 2015. The climate hazards group infrared precipitation with stations (CHIRPS) v2. 0 dataset: 35 year quasi-global precipitation estimates for drought monitoring. AGU Fall Meeting Abstracts, NH41D-05.

Qu, S., Wang, L., Lin, A., Yu, D., Yuan, M., 2020. Distinguishing the impacts of climate change and anthropogenic factors on vegetation dynamics in the Yangtze River Basin, China. Ecological Indicators 108, 105724. https://doi.org/10.1016/j.ecolind.2019.105724

Qu, S., Wang, L., Lin, A., Zhu, H., Yuan, M., 2018. What drives the vegetation restoration in Yangtze River basin, China: climate change or anthropogenic factors? Ecological Indicators 90, 438-450. https://doi.org/10.1016/j.ecolind.2018.03.029

Rannow, S., Neubert, M., 2014. Managing protected areas in central and eastern Europe under climate change. Springer Nature https://doi.org/10.1007/978-94-007-7960-0

Rouse, J.W., Haas, R.H., Schell, J.A., Deering, D.W., 1974. Monitoring vegetation systems in the Great Plains with ERTS. NASA Spec. Publ. 351, 309.

Rousta, I., Mansourmoghaddam, M., Olafsson, H., Krzyszczak, J., Baranowski, P., Zhang, H., *et al*., 2022. Analysis of the recent trends in vegetation dynamics and its relationship with climatological factors using remote sensing data for Caspian Sea watersheds in Iran. Int. Agrophys. 36, 139-153. https://doi.org/10.31545/intagr/150020

Running, S.W., Loveland, T.R., Pierce, L.L., Nemani, R.R., Hunt Jr, E.R., 1995. A remote sensing based vegetation classification logic for global land cover analysis. Remote Sensing Environ. 51, 39-48. https://doi.org/10.1016/0034-4257(94)00063-S

Şahin, M., 2012. Modelling of air temperature using remote sensing and artificial neural network in Turkey. Advances Space Res. 50, 973-985. https://doi.org/10.1016/j.asr.2012.06.021

Şahin, M., Kaya, Y., Uyar, M., 2013. Comparison of ANN and MLR models for estimating solar radiation in Turkey using NOAA/AVHRR data. Advances Space Res. 51, 891-904. https://doi.org/10.1016/j.asr.2012.10.010

Şahin, M., Kaya, Y., Uyar, M., Yıldırım, S., 2014. Application of extreme learning machine for estimating solar radiation from satellite data. Int. J. Energy Res. 38, 205-212. https://doi.org/10.1002/er.3030

Şenkal, O., 2010. Modeling of solar radiation using remote sensing and artificial neural network in Turkey. Energy 35, 4795-4801. https://doi.org/10.1016/j.energy.2010.09.009

Sun, L., Wang, X., Zheng, Y., Wu, Z., Fu, L., 2024. Multiscale 3-d-2-d mixed cnn and lightweight attention-free transformer for hyperspectral and lidar classification. IEEE Trans. Geosci. Remote Sensing 62, 1-16. https://doi.org/10.1109/TGRS.2024.3367374

Tang, X., Cui, Y., Li, N., Fu, Y., Liu, X., Run, Y., *et al*., 2020. Human activities enhance radiation forcing through surface albedo associated with vegetation in Beijing. Remote Sensing 12, 837. https://doi.org/10.3390/rs12050837

Tucker, C.J., Choudhury, B.J., 1987. Satellite remote sensing of drought conditions. Remote Sensing Environ. 23, 243-251. https://doi.org/10.1016/0034-4257(87)90040-X

Wan, Z., 1999. MODIS Land-Surface Temperature Algorithm Basis Document (LST ATBD): version 3.3. http://modis.gsfc.nasa.gov/data/atbd

Wan, Z., Zhang, Y., Zhang, Q., Li, Z.-L. 2002. Validation of the land-surface temperature products retrieved from Terra

Moderate Resolution Imaging Spectroradiometer data. Remote Sensing Environ. 83, 163-180. https://doi.org/10.1016/S0034-4257(02)00093-7

Wang, Y., Quan, S., Tang, X., Hosono, T., Hao, Y., Tian, J., *et al*., 2024. Organic and inorganic carbon sinks reduce long-term deep carbon emissions in the continental collision margin of the southern Tibetan Plateau: Implications for Cenozoic climate cooling. J. Geophys. Res.: Solid Earth 129, e2024JB028802. https://doi.org/10.1029/2024JB028802

Wu, Z., Dijkstra, P., Koch, G.W., Peñuelas, J., Hungate, B.A., 2011. Responses of terrestrial ecosystems to temperature and precipitation change: A meta-analysis of experimental manipulation. Global Change Biol. 17, 927-942. https://doi.org/10.1111/j.1365-2486.2010.02302.x

Xie, D., Huang, H., Feng, L., Sharma, R.P., Chen, Q., Liu, Q., *et al*., 2023. Aboveground biomass prediction of arid shrub-dominated community based on airborne Lidar through parametric and nonparametric methods. Remote Sensing 15, 3344. https://doi.org/10.3390/rs15133344

Xu, J., Zhou, G., Su, S., Cao, Q., Tian, Z., 2022. The development of a rigorous model for bathymetric mapping from multi-spectral satellite-images. Remote Sensing 14, 2495. https://doi.org/10.3390/rs14102495

Xu, L., Myneni, R., Chapin Iii, F., Callaghan, T.V., Pinzon, J., Tucker, C.J., *et al*., 2013. Temperature and vegetation seasonality diminishment over northern lands. Nature Climate Change 3, 581-586. https://doi.org/10.1038/nclimate1836

Yin, G., Hu, Z., Chen, X., Tiyip, T., 2016. Vegetation dynamics and its response to climate change in Central Asia. J. Arid Land 8, 375-388. https://doi.org/10.1007/s40333-016-0043-6

Yin, L., Wang, L., Li, T., Lu, S., Tian, J., Yin, Z., *et al*., 2023a. U-Net-LSTM: time series-enhanced lake boundary prediction model. Land 12, 1859. https://doi.org/10.3390/land12101859

Yin, L., Wang, L., Li, T., Lu, S., Yin, Z., Liu, X., *et al*., 2023b. U-Net-STN: A novel end-to-end lake boundary prediction model. Land 12, 1602. https://doi.org/10.3390/land12081602

Yu, B., Zhou, X., 2024. Land finance and urban Sprawl: Evidence from prefecture-level cities in China. Habitat Int. 148, 103074. https://doi.org/10.1016/j.habitatint.2024.103074

Yuan, Z., Xu, J., Chen, J., Wang, Y., Yin, J., 2022. EVI indicated spatial-temporal variations in vegetation and their responses to climatic and anthropogenic factors in the Chinese Mainland since 2000s. J. Environ. Informatics 40.

Zhang, D., Wu, F., Fang, Y., Lu, N., 2020a. Spatial and temporal variation Trend Analysis of vegetation cover in Urban agglomeration of Pearl River Delta from 2000 to 2015. IOP Conf. Series: Earth Environ. Sci., IOP Publishing 012028. https://doi.org/10.1088/1755-1315/615/1/012028

Zhang, Y.-X., Wang, Y.-K., Fu, B., Dixit, A.M., Chaudhary, S., Wang, S., 2020b. Impact of climatic factors on vegetation dynamics in the upper Yangtze River basin in China. J. Mountain Sci. 17, 1235-1250. https://doi.org/10.1007/s11629-019-5649-7

Zhang, Y., Liang, S., Xiao, Z., 2020c. Observed vegetation greening and its relationships with cropland changes and climate in China. Land 9, 274. https://doi.org/10.3390/land9080274

Zhang, J., Wang, S., Huang, J., He, Y., Ren, Y., 2023. The precipitation-recycling process enhanced extreme precipitation in Xinjiang, China. Geophysical Res. Letters 50, e2023GL104324. https://doi.org/10.1029/2023GL104324

Zhang, K., Li, Y., Yu, Z., Yang, T., Xu, J., Chao, L., Ni, J., Wang, L., Gao, Y., Hu, Y., 2022. Xin'anjiang nested experimental watershed (XAJ-NEW) for understanding multiscale water cycle: scientific objectives and experimental design. Engineering 18, 207-217. https://doi.org/10.1016/j.eng.2021.08.026

Zhang, X., Jin, X., 2021. Vegetation dynamics and responses to climate change and anthropogenic activities in the Three-River Headwaters Region, China. Ecological Indicators 131, 108223. https://doi.org/10.1016/j.ecolind.2021.108223

Zhang, Y., Gao, J., Liu, L., Wang, Z., Ding, M., Yang, X., 2013. NDVI-based vegetation changes and their responses to climate change from 1982 to 2011: A case study in the Koshi River Basin in the middle Himalayas. Global Planetary Change 108, 139-148. https://doi.org/10.1016/j.gloplacha.2013.06.012

Zhao, Y., Li, J., Tian, Y., Li, J., 2024. Distinguish extreme precipitation mechanisms associated with atmospheric river and non-atmospheric river in the Lower Yangtze River Basin. J. Climate. https://doi.org/10.1175/JCLI-D-23-0400.1

Zhou, G., Lin, G., Liu, Z., Zhou, X., Li, W., Li, X., Deng, R., 2023a. An optical system for suppression of laser echo energy from the water surface on single-band bathymetric LiDAR. Optics Lasers Eng. 163, 107468. https://doi.org/10.1016/j.optlaseng.2022.107468

Zhou, G., Zhang, H., Xu, C., Zhou, X., Liu, Z., Zhao, D., Lin, J., Wu, G., 2023b. A real-time data acquisition system for single-band bathymetric LiDAR. IEEE Trans. Geosci. Remote Sensing 61, 1-21. https://doi.org/10.1109/TGRS.2023.3282624

Zhou, Y., Peng, J., Zhang, Z., Li, Y., Cheng, L., 2024. Evaluation and obstacle factors diagnosis of Agriculture Green Development level in China's Yangtze River Basin based on the DPSIR framework. Environ. Develop. Sustain. https://doi.org/10.1007/s10668-024-04467-y

Zhu, Z., Piao, S., Myneni, R.B., Huang, M., Zeng, Z., Canadell, J.G., Ciais, P., Sitch, S., Friedlingstein, P., Arneth, A., 2016. Greening of the Earth and its drivers. Nature Climate Change 6, 791-795. https://doi.org/10.1038/nclimate3004